RADIAL MOISTURE PROFILES OF CEDAR SAPWOOD DURING DRYING: A PROTON MAGNETIC RESONANCE STUDY

Jeff J. Quick
Research Associate
Department of Physics
The University of British Columbia
6224 Agriculture Road
Vancouver, B.C. V6T 2A6, Canada

Joseph R. T. Hailey[1]
Research Scientist
Forintek Canada Corp.
6620 N.W. Marine Drive
Vancouver, B.C. V6T 1X2, Canada

and

Alexander L. MacKay
Assistant Professor
Department of Physics
The University of British Columbia
6224 Agriculture Road
Vancouver, B.C. V6T 2A6, Canada

(Received January 1989)

ABSTRACT

The drying of 6 × 6 × 10 mm western red cedar (*Thuja plicata* Donn.) sapwood samples has been studied with proton magnetic resonance (^{1}H-NMR) imaging. Bulk moisture content and one-dimensional radial moisture profiles have been observed as functions of time under controlled air flow rate and temperature conditions. The effects of these drying conditions on the behavior of bulk moisture content with time corresponded well to the effects observed in full-scale lumber drying, although typical observed drying rates were of the order of 100 times faster. Sub-millimeter resolution of the radial water distribution has been attained with moisture contents from the green state to as low as a few percent, and contrasting drying behavior has been observed in the earlywood and latewood regions of the growth rings.

Keywords: Cedar, sapwood, drying, proton magnetic resonance, imaging, moisture profiles, moisture content.

INTRODUCTION

Proton Magnetic Resonance (^{1}H-NMR) has been shown (Menon et al. 1987, 1989) to provide the most direct and detailed information on water in wood, specifically:

(a) The water ^{1}H-NMR signal is easily separable from the much broader line ^{1}H-NMR signal of the wood;

---

[1] Currently at 1273 Clyde Ave, West Vancouver, B.C. V7T 1E6, Canada

Wood and Fiber Science, 22(4), 1990, pp. 404–412

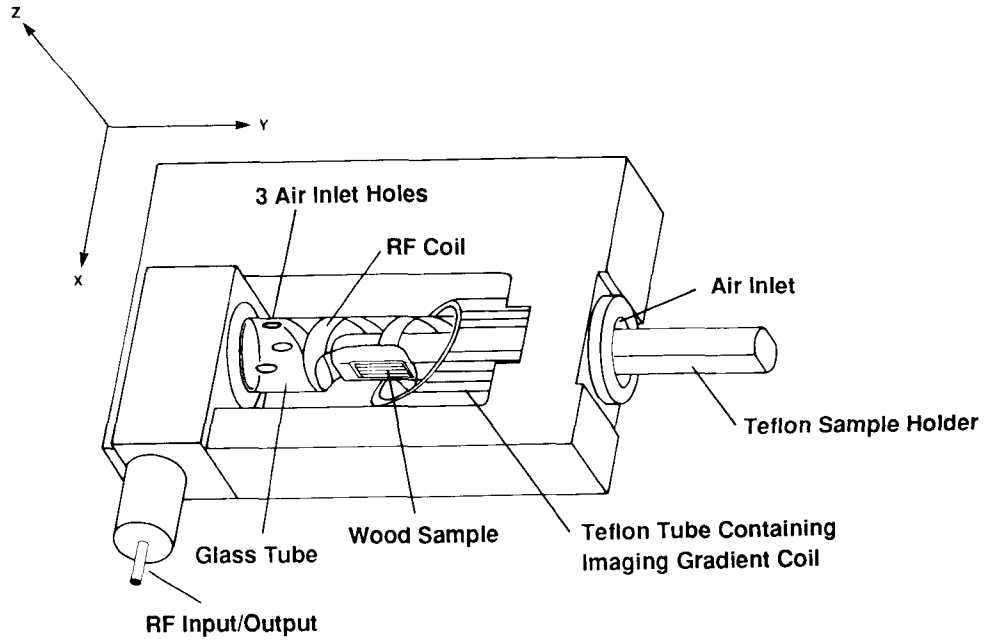

FIG. 1. NMR Probe containing the 6 × 6 × 10 mm wood sample.

(b) Accurate determination of bulk moisture content (MC) is possible;

(c) A one-dimensional imaging technique in a solid state spectrometer provides valuable spatial information with sub-millimeter resolution.

In this study, ^{1}H-NMR has been used to determine MC and image the total water distribution in western red cedar (*Thuja plicata* Donn.) sapwood samples, hereafter called "cedar," during continuous drying.

The Nuclear Magnetic Resonance (NMR) technique is based on the fact that nuclei with magnetic moments and angular momenta will absorb energy in a resonant manner, at a frequency proportional to the local magnetic field strength. Imaging techniques use linear magnetic field gradients to map position into the frequency domain. For the relatively small wood samples studied here, a single gradient was used to make one-dimensional images of the water distribution in the radial direction.

The wood drying method consisted of controlling the entering air flow rate and temperature. The flow was non-recirculating and inlet humidity was constant over the course of an experiment. This method is in contrast to commercial kiln operation where the lumber charge is much larger and schedules involve strict control of dry-bulb and wet-bulb temperatures and air flow velocity, usually as functions of time or MC readings.

EXPERIMENTAL

Wood samples

Four 6 × 6 × 10 mm cedar sapwood samples were cut from a fresh cut log cross-section with the 10 mm dimension parallel to the longitudinal tracheids.

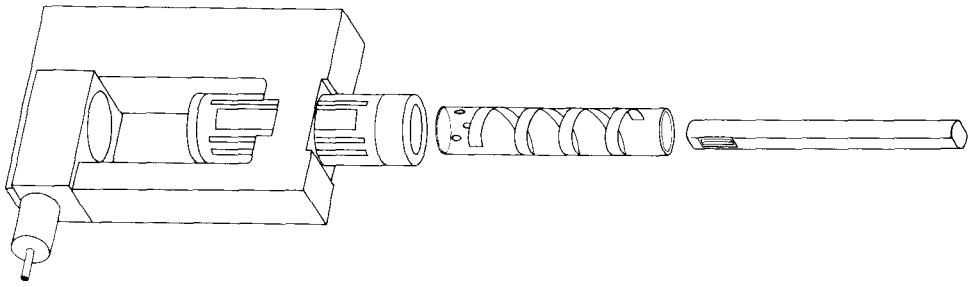

FIG. 2. Exploded view of the NMR probe.

The samples were weighed prior to being placed in the spectrometer so initial MCs could be determined by the oven-dry method. Scanning Electron Micrographs (SEM) were made of cross-sections of the dry samples. The specific gravity of each sample was determined by the maximum moisture content method of Smith (1954) in order to scale radial moisture profile data to water density.

Wood drying chamber

The NMR probe that contained the wood sample is shown in Figs. 1 and 2. The sample was placed in a teflon holder inside a 9.5 mm id glass tube. It was arranged such that the tangential direction of the growth rings was parallel to the X-axis of the indicated coordinate system, and the radial direction was parallel to the Z-axis. Air flow passed downward between the outer teflon and inner glass tubes, through three holes around the perimeter at the base of the glass tube and back up the inside past the sample. The sample holder lightly gripped the tangential faces leaving the two radial faces directly exposed to air flow. The cross-sectional faces were partially exposed.

The air flow path around the sample is quite complex, so that velocity profiles would be difficult to predict. In particular, the inlet conditions will introduce turbulent mixing, notwithstanding typically low average Reynolds numbers of order 100; and there is a significant contraction of the flow path cross-sectional area around the sample holder. For these reasons, comparison of volume flow rates rather than velocities is made between various runs.

NMR measurements

All NMR measurements were made using a modified Bruker SXP 4-100 spectrometer operating at 90 MHz. Data acquisition and analysis were carried out

TABLE 1. *Drying conditions and observed specific drying rates (see Fig. 4)*

Run	Drying conditions		MC range over which specific drying rate determined (%)	Specific drying rate k (h^{-1})
	Inlet air flow rate (l/h)	Temperature (°C)		
1	10	26	98–30	1.8
			30–3.1	1.3
2	5	26	99–4.2	1.3
3	5	37	67–2.0	2.1
4	8	47	33–1.0	4.9

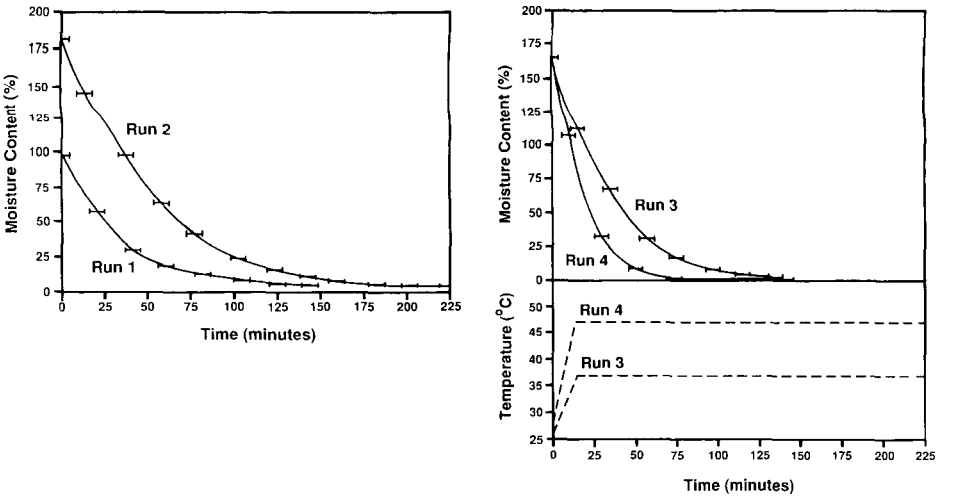

FIG. 3a. Drying curves for run 1 (10 l/h, 26 C) and run 2 (5 l/h, 26 C) plotted as moisture content versus time. Bars indicate data collection intervals.

FIG. 3b. Drying curves for run 3 (5 l/h) and run 4 (8 l/h) plotted as moisture content versus time, with temperature plotted below these curves. Bars indicate data collection intervals.

with a self-contained system (Sternin 1985) including a MicroVax II and a National 32016 computer, a Nicolet 2090 digital oscilloscope, and locally built pulse programmer.

The magnetic field gradient used was 19.4 gauss/cm oriented in the Z-direction as indicated in Fig. 1, which is the radial direction of the wood sample. The RF pulse sequence consisted of a $90°_y$ followed by a $180°_x$ pulse to refocus the signal to a Hahn echo. The delay between excitation and echo was 400 μsec to ensure no contribution from the unwanted solid wood ^1H signal which generally decayed in about 50 μsec. The free induction decay (FID) from the echo peak was digitized with a 5 μsec dwell time for a total of 2,048 complex points.

Signal averaging of at least 100 scans improved signal to noise of the resulting FIDs. This resulted in data collection intervals of at least 8 minutes. Every second scan contained a 90° pulse shifted in phase by 180° and was subtracted from the cumulative sum to reduce coherent noise and to offset errors over the course of an FID collection. The repetition time between scans was 5 sec to allow return of the spin system to thermal equilibrium (i.e., sufficiently longer than spin-lattice relaxation time, T_1).

Drying runs

Each of the four wood samples was dried in the chamber under the air flow and temperature conditions presented in Table 1. An initial FID was collected for each run, and the resulting Hahn echo amplitude was assigned to the initial bulk MC, as determined by the oven-dry method, in order to scale all subsequent data to bulk MC. Following the initial FID collection air flow was turned on. Runs 1 and 2 were carried out at 26 C. For runs 3 and 4 the entering air temperature was rapidly raised to 37 and 47 C, respectively, and held constant by a Bruker B-ST 100/700 temperature controller.

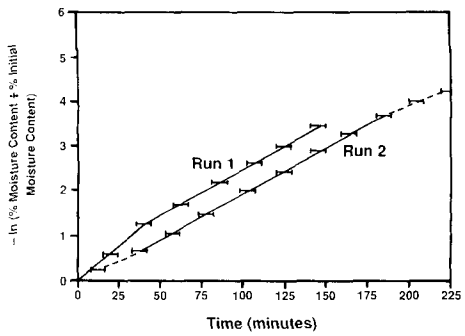

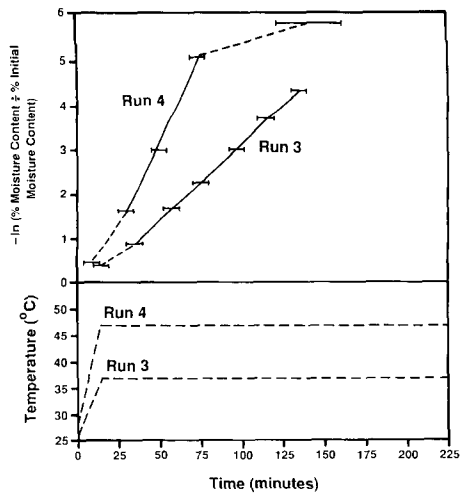

FIG. 4a. Drying curves for run 1 (10 l/h, 26 C) and run 2 (5 l/h, 26 C) plotted as negative logarithm normalized moisture content versus time. The slopes of the curves are the specific drying rates (see Table 1). Bars indicate data collection intervals.

FIG. 4b. Drying curves for run 3 (5 l/h) and run 4 (8 l/h) plotted as negative logarithm normalized moisture content versus time with temperature plotted below these curves. The slopes of the curves are the specific drying rates (see Table 1). Bars indicate data collection intervals.

RESULTS AND DISCUSSION

Drying curves

The drying curves for each of the four cedar sapwood samples are plotted as MC vs. time in Figs. 3a and 3b. The inlet air flow rates and temperature for each are also included with these plots, and data collection intervals are indicated by horizontal bars. Typical drying times for these small samples were about 100 times shorter than for conventional, low temperature schedule, commercial kiln drying of softwoods. The data have also been plotted logarithmically in Figs. 4a and 4b as $-\ln$(% Moisture Content ÷ % Initial Moisture Content) versus time. The slopes of the linear regions (solid lines) of the curves give the specific drying rates (k), as discussed by Salamon and McIntyre (1969) in reference to Dedrick (1968). While this form does not provide a particularly good model of the overall drying process, it is useful for comparing runs made under different conditions of air flow and temperature. A summary of key results is presented in Table 1.

Comparison of runs 1 and 2 (Table 1) indicates that doubling air flow rate has increased the specific drying rate by approximately 30% at MCs above the fiber saturation point (FSP) (about 30%) and had no measurable effect below the FSP. This agrees with results of Salamon and McIntyre (1969), who found that increasing air velocity from 400 ft/min to 600 ft/min and 900 ft/min, under constant kiln/charge geometry, increased drying rate at MCs above 25% but had little or no effect below 25% MC for three softwood species: western hemlock, western white spruce and Douglas-fir.

Furthermore, it is generally understood that the mechanisms of drying above the FSP involve capillary movement and evaporation of lumen water, whereas

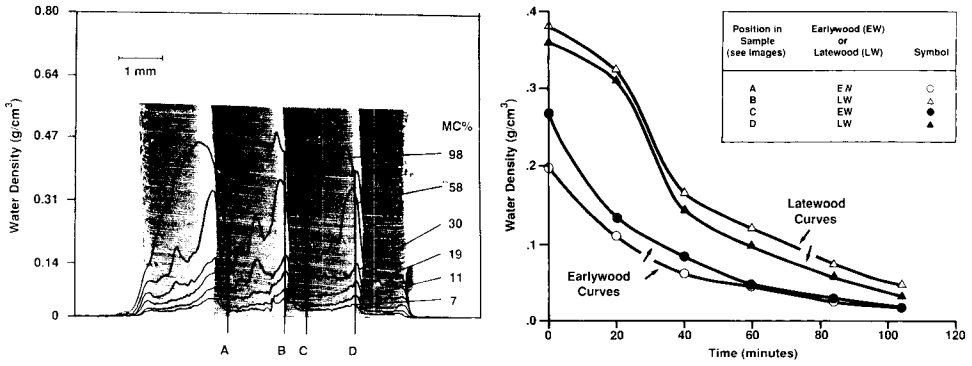

FIG. 5a. Run 1: NMR images of the radial moisture profiles during drying superimposed on the cross-sectional scanning electron micrograph.

FIG. 5b. Run 1: Earlywood (A, C) and latewood (B, D) drying curves obtained at positions A, B, C and D of Fig. 5a.

at lower MC vapor and bound water diffusion dominate. The former should depend strongly on volume flow rate of air to carry away evaporated moisture. Bound water diffusion has been described in terms of gradients in MC, vapor pressure, temperature, chemical potential, and spreading pressure (Nelson 1986) as the driving forces, which should not depend strongly on air flow rate. Also, the flux of water associated with this stage of drying is much smaller than it is above the FSP so that as long as the air flow rate is sufficient to remove this water, increasing the air flow rate should not remove this water any faster.

Comparison of runs 2 and 3 (Table 1) shows that raising the temperature from 26 to 37 C increased the specific drying rate by 60% both above and below the FSP. Above the FSP, the removal of capillary water is expected to become faster because the air carries more heat for evaporation, the lower relative humidity of the heated air enables it to carry away more moisture, and water viscosity decreases with higher temperature so that liquid water may be moved more easily through

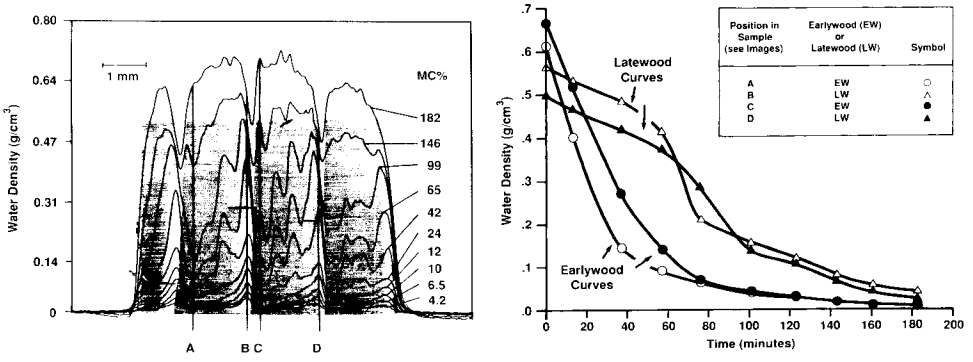

FIG. 6a. Run 2: NMR images of the radial moisture profiles during drying superimposed on the cross-sectional scanning electron micrograph.

FIG. 6b. Run 2: Earlywood (A, C) and latewood (B, D) drying curves obtained at positions A, B, C and D of Fig. 6a.

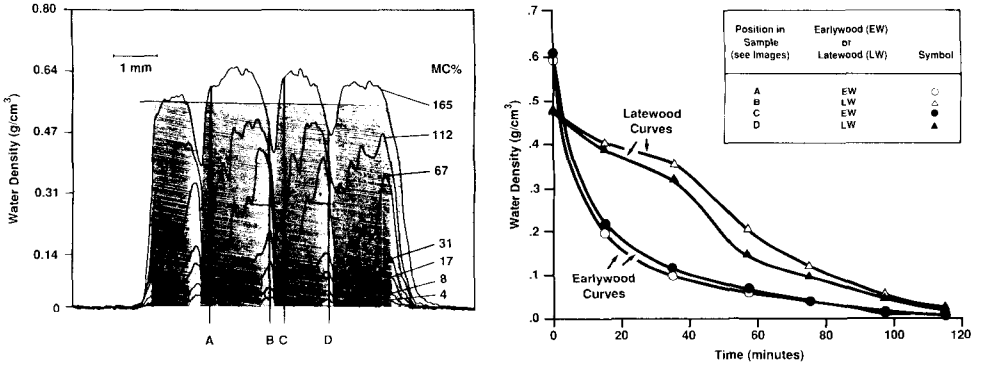

FIG. 7a. Run 3: NMR images of the radial moisture profiles during drying superimposed on the cross-sectional scanning electron micrograph.

FIG. 7b. Earlywood (A, C) and latewood (B, D) drying curves obtained at positions A, B, C and D of Fig. 7a.

pit openings by capillary forces. Below the FSP, the higher temperature should raise diffusion rates. It may only be coincidence that the rate is increased here by the same amount both above and below the FSP.

Run 4 (Table 1) was carried out at a much higher temperature of 47 C and a high air flow rate of 8 l/h. If one compares data at MCs below the FSP (Table 1), where the air flow rate is presumed to have little effect, it is evident that the 10 C temperature rise from 37 C in run 3 to 47 C in run 4 has resulted in a 130% increase in specific drying rate.

One-dimensional images

The Fourier transform (FT) of the FID is the one-dimensional image of the radial moisture profile with amplitude proportional to number of water protons at a particular frequency or corresponding position. Using the results of the wood specific gravity measurements, the image amplitude was scaled to water density based on green sample volume. Theoretical spatial resolution has been estimated at 50 μm. One is most interested in comparison of the water distribution to the wood anatomy, however, and it is the latter which determines the finest resolution to which one should expect to make such comparisons. The obvious indicators of this are the deviations from linearity of the earlywood/latewood boundaries between growth rings. The images collected for each sample are presented with SEMs through cross-sections of each for comparison in Figs. 5a, 6a, 7a and 8a.

The annual growth pattern of the tree is clearly identifiable in the images. At MCs below the FSP, the remaining moisture is predominantly bound within the cell wall. The radial moisture profiles indicate an increase in the bound water density corresponding to the increase in wood density from earlywood to latewood. These low MC images identify the boundaries between growth rings and show good correspondence to the SEMs of the samples. In the green state (Figs. 6a, 7a and 8a), there are dips in the water density profiles in the latewood area as expected since there is less void volume for the water to occupy. The images also exhibit anomalous oscillations in water density which do not correlate with anything structural on the SEMs.

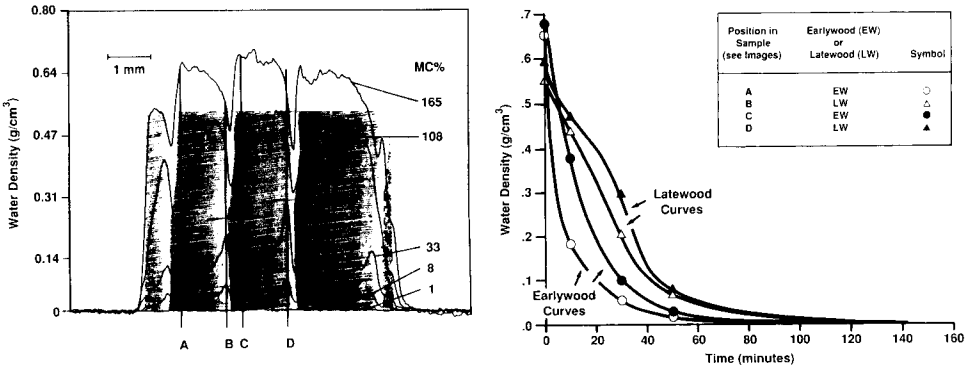

FIG. 8a. Run 4: NMR images of the radial moisture profiles during drying superimposed on the cross-sectional scanning electron micrograph.

FIG. 8b. Earlywood (A, C) and latewood (B, D) drying curves obtained at positions A, B, C and D of Fig. 8a.

From the image data, earlywood and latewood drying curves were constructed for specific points in the earlywood and latewood regions of the growth rings (Figs. 5b, 6b, 7b and 8b). There is clearly a distinction between the behavior in these two regions of a growth ring. During the initial stages of drying, the latewood dries at a slower rate. This could be due in part to a lower water potential associated with the smaller tracheid lumen size of the latewood, as described by Siau (1984). There follows an intermediate stage where the latewood drying rate becomes very rapid, with the bulk MC still above the FSP. The earlywood curves show a smoother falling drying rate. Below the FSP both earlywood and latewood exhibit similar drying rates with the latewood having a higher water density.

SUMMARY

^{1}H-NMR is an effective new method for observing continuous wood drying because the water signal is separable from that of the wood and is linearly proportional to water content. Images of the water distribution can be obtained with sub-millimeter resolution.

The four 6 × 6 × 10 mm samples, each containing about four growth rings, dried about 100 times faster than typical commercial softwood kiln charges dried under conventional, low temperature schedules. Increasing air velocity raised the specific drying rate at MCs above the FSP where removal of capillary water is dominant, but had no effect below the FSP where bound water diffusion is dominant. Increasing temperature raised specific drying rate at all MCs. These flow and temperature effects are typical of those observed in full scale kiln drying.

The NMR images obtained demonstrate the capability of the method to resolve the radial moisture profiles in wood during continuous drying. These data show that water removal as a function of time differs in the earlywood and latewood. This type of information about the moisture distribution in wood during drying has not previously been available to lumber drying researchers and emphasizes the potential of NMR for further research into the physical mechanisms of wood drying.

ACKNOWLEDGMENTS

The authors wish to thank the Canadian Forestry Service, the Natural Sciences and Engineering Research Council of Canada, and the Engineering Physics Project Laboratory* at the University of British Columbia for providing support for this work. The authors also wish to thank J. F. G. Mackay for comments made during the writing of this paper.

REFERENCES

DEDRICK, D. S. 1968. Some observations of the kinetics of lumber drying in conventional kilns. Proc. 19 Annual Meeting, Western Dry Kiln Clubs. Pp. 5–11.

MENON, R. S., A. L. MACKAY, J. R. T. HAILEY, M. BLOOM, A. E. BURGESS, AND J. S. SWANSON. 1987. An NMR determination of the physiological water distribution in wood during drying. J. Appl. Polym. Sci. 33:1141–1155.

———, ———, S. FLIBOTTE, AND J. R. T. HAILEY. 1989. Quantitative separation of NMR images of water in wood on the basis of T_2. J. Magn. Res. 82:205–210.

NELSON, R. M., JR. 1986. Diffusion of bound-water in wood, Part I: The driving force. Wood Sci. Technol. 20(2):125–135.

SALAMON, M., AND S. MCINTYRE. 1969. Manipulation of air velocity permits drying time savings. Report from Canadian Forest Industries (September 1969).

SIAU, JOHN F. 1984. Transport processes in wood. Springer-Verlag, Berlin, New York. 131 p.

SMITH, D. M. 1954. Maximum moisture content method for determining specific gravity of small wood samples. Forest Products Laboratory, Madison, WI. Report No. 2014. 8 pp.

STERNIN, E. 1985. Data acquisition and processing: A systems approach. Rev. Sci. Instrum. 56(11): 2043–2049.

* Supported by the Funds for Excellence in Education Program of the Ministry of Advanced Education and Job Training.